ENVIRONMENTAL RESEARCH
CLIMATE

Ultrafast Arctic amplification and its governing mechanisms

To cite this article before publication: Tyler P Janoski *et al* 2023 *Environ. Res.: Climate* in press https://doi.org/10.1088/2752-5295/ace211

Ultrafast Arctic Amplification and Its Governing Mechanisms

Tyler P. Janoski[1,2], **Michael Previdi**[2], **Gabriel Chiodo**[3], **Karen L. Smith**[2,4] **and Lorenzo M. Polvani**[1,2,5]

[1] Department of Earth and Environmental Sciences, Columbia University, New York, NY, USA

[2] Lamont-Doherty Earth Observatory, Palisades, NY, USA

[3] ETH Zürich, Zürich, Switzerland

[4] Department of Physical and Environmental Sciences, University of Toronto Scarborough, Scarborough, ON, Canada

[5] Department of Applied Physics and Applied Mathematics, Columbia University, New York, NY, USA

Abstract

Arctic amplification (AA), defined as the enhanced warming of the Arctic compared to the global average, is a robust feature of historical observations and simulations of future climate. Despite many studies investigating AA mechanisms, their relative importance remains contested. In this study, we examine the different timescales of these mechanisms to improve our understanding of AA's fundamental causes. We use the Community Earth System Model v1, Large Ensemble configuration (CESM-LE), to generate large ensembles of 2-year simulations subjected to an instantaneous quadrupling of CO_2. We show that AA emerges almost immediately (within days) following CO_2 increase and before any significant loss of Arctic sea ice has occurred. Through a detailed energy budget analysis of the atmospheric column, we determine the time-varying contributions of AA mechanisms over the simulation period. Additionally, we examine the dependence of these mechanisms on the season of CO_2 quadrupling.

We find that the surface heat uptake resulting from the different latent heat flux anomalies between the Arctic and global average driven by the CO_2 forcing, is the most important AA contributor on short (< 1 month) timescales when CO_2 is increased in January, followed by the lapse rate feedback. The latent heat flux anomaly remains the dominant AA mechanism when CO_2 is increased in July and is joined by the surface albedo feedback, although AA takes longer

to develop. Other feedbacks and energy transports become relevant on longer (> 1 month) timescales. Our results confirm that AA is an inherently fast atmospheric response to radiative forcing and reveal a new AA mechanism.

1. Introduction

Arctic amplification (AA), or the enhanced surface warming of the Arctic relative to the global mean, is a ubiquitous feature of anthropogenic climate change. First predicted by Arrhenius in 1896 as a response to increasing CO_2 (Arrhenius, 1896), AA has since consistently appeared in climate model simulations (e.g., Manabe & Stouffer, 1980; Hwang et al., 2011; Pithan & Mauritsen, 2014) and observations (e.g., Serreze et al., 2009; Cohen et al., 2014; Wang et al., 2016). The local and global importance of AA cannot be overstated. The Arctic is home to ~4 million people, including indigenous peoples who have lived there for 20,000 years (National Snow & Ice Data Center, 2020). Amplified Arctic warming threatens these peoples' ways of life while simultaneously endangering the surrounding Arctic ecosystems (Meltofte et al., 2013; Moon et al., 2021). Impacts of AA are not limited to the Arctic; a warmer Arctic may lead to the release of methane, a potent greenhouse gas (GHG), from permafrost (Zubrzycki et al., 2014) and may influence extreme weather in the midlatitudes (Francis & Vavrus, 2012; Cohen et al., 2014, Smith et al., 2022). There may, however, be some benefits to global shipping and agriculture from Arctic warming (Ho, 2010; Altdorff et al., 2021).

Despite AA's ubiquity, the question of the mechanisms to which AA owes its existence remains open, limiting our ability to understand and accurately project future Arctic climate. Some studies have emphasized the role of local feedbacks over the Arctic, which may enhance or diminish an initial temperature response; these include temperature feedbacks (Winton, 2006; Pithan & Mauritsen, 2014; Stuecker et al., 2018), the surface albedo feedback (Holland & Bitz, 2003; Screen & Simmonds 2010; Dai, 2021), and cloud feedbacks (Vavrus et al., 2011; Cao et al., 2017; Jenkins & Dai, 2022). Others attribute AA mainly to changes in heat transport into the Arctic by the atmosphere, specifically through enhanced moisture transport (Lee, 2014; Merlis & Henry, 2018; Graversen & Langen, 2019; Russotto & Biasutti, 2020) and the ocean (Bitz et al., 2006; Singh et al., 2017; van der Linden et al., 2019). This issue is further complicated by the coupling between different local feedbacks or energy transports, which may obscure the effect of individual contributions to AA (Hwang et al., 2011; Graversen et al., 2014; Feldl et al., 2017; Chung et al., 2021; Previdi et al., 2021). For example, although the lapse rate feedback, a type of temperature feedback, is often considered in isolation, it is strongly linked to sea ice loss, atmospheric heat transport, and surface temperature response (Feldl et al., 2020; Boeke et al., 2021).

It is important to note that these proposed AA mechanisms operate on different timescales, mainly because of the different rates with which climate system components respond to radiative forcing. However, most previous studies of AA do not discriminate between these different timescales and focus on the long-term (e.g., multi-decadal) or equilibrium response to an imposed forcing. An exception to this is the recent study of Previdi et al. (2020), which focused specifically on the different timescales of AA. In that study, a collection of models from the Coupled Model Intercomparison Project phase 5 (CMIP5) subjected to an instantaneous quadrupling of CO_2 relative to preindustrial levels was analyzed, and the contributions of different AA mechanisms were quantified. It was shown that the relative importance of various mechanisms depends on the timescale; for example, the lapse rate feedback is the main contributor to AA across CMIP5 models in the first three months following the CO_2-quadrupling, but in the last 30 years of the simulations (representing the quasi-equilibrium response), the surface albedo feedback dominates (Previdi et al., 2020). Thus, to elucidate the relative contributions of different mechanisms to AA, one must pay careful attention to the timescale being considered. The main conclusion of Previdi et al. (2020) is that AA is inherently a rapid response to radiative forcing, fundamentally owing its existence to fast atmospheric processes.

Although an important first step, the study by Previdi et al. (2020) was hampered by several factors. First, only 21 CMIP5 models provided the variables necessary to complete an energy budget analysis. This relatively small sample size made it difficult to robustly characterize the evolution of AA, particularly on the short timescales of interest where internal variability (especially in the Arctic) is large. Second, CMIP5 output was only available as monthly means. This precluded any assessment of the role of sub-monthly processes in AA. Given the rapid timescale associated with AA, the coarse time resolution of the data and the lack of multiple realizations posed a key limitation to their conclusions based on CMIP5 data. Finally, all simulations analyzed in that study had CO_2 quadrupling on January 1st, leaving open the question of how the time evolution of AA would differ if CO_2 were quadrupled in different seasons. Bintanja & Krikken (2016) previously explored the impact of the season of CO_2 forcing on Arctic warming, but at timescales beyond the initial response. The timing of CO_2 increase is particularly important in the Arctic, which cycles through 6-month polar days and nights, experiencing a very large seasonal cycle.

Here, we seek to overcome these limitations and build upon the work of Previdi et al. (2020) by analyzing the development of AA using high-frequency (daily) output from climate model simulations subjected to an instantaneous quadrupling of CO_2. To address the small signal-to-noise ratio of the Arctic (Screen et al., 2014; Swart et al., 2015; England et al., 2019), we generate two large ensembles of simulations (50-100 members) in which CO_2 is increased at different times during the year (either January or July). The questions we seek to answer are as follows:

- How quickly does AA develop in an ensemble of model simulations subjected to an instantaneous CO_2 increase?
- What mechanisms best explain the initial appearance and the subsequent evolution of AA?
- How does the time of year in which atmospheric CO_2 is quadrupled affect AA development?

2. Methods

2.1 Model Description

In this study, we used the Community Earth System Model, Large Ensemble configuration (CESM-LE). CESM-LE is a fully coupled global climate model (GCM) based on version 1.1.1 of the Community Earth System Model (CESM), a model included in CMIP5, and has active atmosphere, land, ocean, and sea ice components. The atmosphere model in CESM-LE is the Community Atmosphere Model version 5 (CAM5), with a horizontal resolution of ~1°. For more detailed information about the CESM-LE configuration, see Kay et al. (2015); for CAM5, see Hurrell et al. (2013).

CESM-LE is well-suited for studies of Arctic climate because of its ability to simulate the modern Arctic sea ice state (Jahn et al., 2016) and its outperformance of other CMIP5 models in capturing the internal variability of Arctic sea ice (England et al., 2019). Consequently, CESM-LE has a strong precedent of use in Arctic climate studies (e.g., Jahn et al., 2016; Labe et al., 2018; Yang & Magnusdottir, 2018).

2.2 Experiment Design

We generated large ensembles of simulations with CESM-LE, with individual ensemble members differing only in their initial conditions. The initial conditions were chosen randomly from an existing ~2200-year-long CESM-LE control simulation with fixed preindustrial forcing available on National Center for Atmospheric Research (NCAR) machines (Kay & Deser, 2016). This initialization approach was chosen to better sample climate state variability in the days following CO_2 increase by ensuring that ensemble realizations are sufficiently different, as opposed to the method used in Kay et al. (2015), in which small round-off level perturbations are introduced to initial conditions. The existing control simulation had restart files available every ~5 years. Our ensembles consist of paired 2-year-long CESM-LE runs. The first run in each pair has fixed preindustrial forcing (piControl), while the second is subjected to an instantaneous CO_2-quadrupling relative to preindustrial levels ($4\times CO_2$).

To investigate the impact of the time of year of $4\times CO_2$ on AA, we created two ensembles, one containing members initialized on January 1st and the other with members initialized on July 1st of the same model year. Because restart files from the existing CESM-LE run were only available for Jan 1st, we generated new restart files for July from our January-initialized piControl simulations. All model output was saved as daily averages.

For the sake of readability, we henceforth refer to the experiment in which CO_2 is quadrupled in January as Jan$4\times CO_2$ and in July as Jul$4\times CO_2$. Jan$4\times CO_2$ and Jul$4\times CO_2$ have 100 and 50 ensemble members, respectively. These ensemble sizes were determined carefully considering the seasonality of Arctic internal variability and computational constraints, along with the suggestion of a 100-member minimum in the Polar Amplification Model Intercomparison Project (Smith et al., 2019). Given the large internal variability in the Arctic region, we ran multiple members to ensure that a forced AA signal could be separated from the variability; we later show results with different ensemble sizes for context.

2.3 Energy Budget Analysis

2.3.1 FRAMEWORK

We compare the global average and Arctic energy budgets to understand how the CO_2 radiative forcing, climate feedbacks, and energy transports contribute to AA. We define the Arctic as the region from 70°N - 90°N, with approximately the same fractional land area as the global average (~0.29). Because of the fast timescales in our analysis, we prefer not to use the ratio of Arctic to global warming to avoid dividing by near-zero global temperature changes. Therefore, we generally define AA and warming contributions to AA as the difference between the Arctic and global averages.

We adopt an energy budget framework similar to that of Pithan & Mauritsen (2014), Goosse et al. (2018), Zhang et al. (2018), and Previdi et al. (2020). We consider an atmospheric column that extends from the top of the atmosphere (TOA) to the surface, with R representing the net downward radiative flux at the TOA. If we introduce a TOA radiative imbalance by subjecting the column to some radiative forcing ΔF, we can relate the imbalance and forcing as follows:

$$\Delta R = \Delta F + \lambda \Delta T_s + \Delta AHT + \Delta SHU \quad (1)$$

where λ is the local climate feedback parameter, T_s is the surface air temperature, AHT is the vertically integrated convergence of the atmospheric heat transport, and SHU is the surface heat uptake, defined as positive upwards (i.e., into the column). Δ represents the difference between the piControl and 4×CO_2 simulations. Because of the short timescales of interest, we take ΔF to be the instantaneous radiative forcing at the TOA from 4×CO_2. We compute this radiative forcing using the Parallel Offline Radiative Transfer (PORT) model with CESM (Conley et al., 2013). Responses to the instantaneous CO_2 forcing that affect ΔR and ΔSHU are generally referred to as "feedbacks" for ease of discussion. However, in Section 4, we consider which of these responses may be more appropriately regarded as "rapid adjustments."

We decompose the net climate feedback parameter λ as follows (Pithan & Mauritsen, 2014; Zhang et al., 2018; Goosse et al., 2018):

$$\lambda = \lambda_o + \sum_x \lambda_x \tag{2}$$

where λ_o is the Planck feedback, and λ_x represents feedbacks due to changes in water vapor, clouds, the atmospheric lapse rate (LR), and surface albedo. Following past studies (Pithan & Mauritsen, 2014; Goosse et al., 2018), we further decompose the Planck feedback into a global mean value $\overline{\lambda_o}$ and local deviation from the global mean, λ_o':

$$\lambda_o = \overline{\lambda_o} + \lambda_o'. \tag{3}$$

The atmospheric heat transport into the Arctic is computed directly from model covariance fields. The meridional flux of moist static energy into the Arctic can be written as follows:

$$AHT = \frac{C}{2\pi A}\int_0^{2\pi}\int_0^{p_s}\frac{v(c_pT + gz + L_vq)dxdp}{g} \tag{4}$$

with A being the area of the Arctic, C the circumference of the southern latitudinal boundary of the Arctic, p_s the surface pressure, v the meridional component of the wind, c_p the specific heat of dry air, T the air temperature, g the gravitational constant, L_v the latent heat of vaporization of water, and q the specific humidity (Cardinale et al., 2021). The global average atmospheric heat transport convergence is zero, by definition.

Because covariance terms involving the zonal component of the wind were not available, we calculate the AHT convergence as a residual when estimating warming contributions separately for land and ocean (see section 5):

$$AHT = \frac{dE}{dt} - SHU - R \tag{5}$$

where $\frac{dE}{dt}$ is the time rate of change in atmospheric column energy, SHU is the surface heat uptake, and R is the net radiative flux at the TOA, as in Eq. 1. The AHT calculated as a residual closely matches the direct calculation (not shown).

The surface heat uptake is equal to the net surface heat flux from the model. It can be decomposed into radiative and non-radiative components; the former includes contributions from surface radiative forcing and feedbacks, and the latter contains sensible and latent heat fluxes:

$$\Delta SHU = \Delta F_{sfc} = \Delta F_{CO_2} + \Delta F_{LH} + \Delta F_{SH} + \Delta T_s \sum_x \lambda_{s,x} \quad (6)$$

F_{sfc} is the net surface heat flux, ΔF_{CO_2} is the instantaneous 4×CO_2 radiative forcing from CESM-PORT at the surface, F_{LH} is the latent heat flux, F_{SH} is the sensible heat flux, and $\lambda_{s,x}$ represents feedbacks at the surface from changes in temperature, water vapor, clouds, and surface albedo. The radiative feedbacks at the surface are mostly analogous to their TOA counterparts in that they quantify radiative perturbations from changes in certain fields at the surface instead of the TOA. As in Eq. 1, SHU and all of its components are defined such that positive values indicate the flow of energy from the surface into the atmospheric column. This sign convention at the surface is opposite to that of Pithan & Mauritsen (2014) and Laîné et al. (2016). We offer two reasons for this difference. First, SHU should be positive and, therefore, contribute to Arctic warming in the fall and winter, when the ocean acts as a heat source to the atmosphere (Screen & Simmonds, 2010; Bintanja & van der Linden, 2013; Boeke & Taylor, 2018; Chung et al., 2021; Dai et al., 2021). Second, on the longer, annual timescales analyzed by Pithan & Mauritsen (2014) and Laîné et al. (2016), energy added to the surface is ultimately realized as surface warming; this is not necessarily true on the fast timescales examined in this study, for which we must account for the storage of heat in the surface.

2.3.2 Feedback calculations

We use the radiative kernel technique to quantify the radiative perturbations at the TOA and surface from climate feedbacks (Soden et al., 2008, Shell et al., 2008). We employ the CAM5 kernels documented in Pendergrass et al. (2018), which have the same horizontal resolution and underlying radiation code as our CESM-LE simulations and were created with CESM 1.1.2 fields (e.g., temperature, moisture, and clouds). The kernels were only available as monthly averages, so they were linearly interpolated with periodic boundary conditions to a daily resolution to match the model output. Height-dependent kernels and model output were linearly regridded from the native hybrid-sigma coordinates to standard pressure levels for feedback calculations.

The TOA temperature feedback was separated into Planck and LR components. For the Planck feedback, a vertically uniform temperature change equal to the surface air temperature change was assumed. The LR feedback was calculated as the departure from this vertically uniform temperature change. We used the change in the natural logarithm of the specific humidity to compute the radiative perturbation due to water vapor feedback (Soden et al., 2008). Tropospheric temperature and water vapor feedbacks are vertically integrated from the surface to the model-defined tropopause. Stratospheric feedbacks are quantified similarly by integrating from the tropopause to the TOA.

The temperature feedback at the surface was decomposed into surface warming and atmospheric warming feedbacks, corresponding to changes in outgoing longwave radiation from the surface and incoming longwave radiation from the atmosphere received by the surface, respectively (Pithan & Mauritsen, 2014).

The cloud feedback (ΔR_{cloud}) is determined using the "adjustment method" developed by Soden et al. (2008). In this method, the change in cloud radiative effect (ΔCRE) is adjusted to remove the effects of cloud masking, i.e.:

$$\Delta R_{cloud} = \Delta CRE - \left(\Delta F - \Delta F^{o}\right) - \sum_{x}\left(\Delta R_{x} - \Delta R_{x}^{o}\right) \tag{7}$$

where ΔF and ΔR_x represent the all-sky radiative perturbations at the TOA or surface due to climate forcing and feedbacks, respectively, and the superscript ^{o} indicates the clear-sky perturbations (e.g., see Zhang et al., 2018).

We express forcing, feedback, and transport terms as warming contributions to the global or Arctic average surface air temperature response, as was done by Crook et al. (2011), Feldl & Roe (2013), Pithan & Mauritsen (2014), Goosse et al. (2018), and Previdi et al. (2020). This is achieved by normalizing each term (in W m^{-2}) by the magnitude of the time-averaged ensemble-mean global Planck feedback (~3.2 W m^{-2} K^{-1}).

3. Rapid AA after 4×CO_2

We begin by observing the evolution of the global and Arctic average SAT response in Jan4×CO_2 (Fig. 1a). AA rapidly develops as the ensemble mean Arctic SAT response quickly diverges from the global average within days after 4×CO_2. In the first week, the ensemble mean Arctic warming is nearly double that of the global average (0.75 K vs. 0.34 K); this difference grows when the first three months are considered (1.69 K vs. 0.68 K), comparable to the Arctic-to-global warming ratio reported in Previdi et al. (2020) over the same timescale. In Jul4×CO_2 (Fig. 1b), it takes longer for the Arctic and global average temperature responses to diverge, corresponding to the well-observed seasonally reduced AA in boreal summer (Lâiné et al., 2016). Even with the slower start in Jul4×CO_2, the Arctic warms considerably more than the global average in the first three months (1.52 K vs. 0.82 K). The pronounced seasonal variability in Arctic SAT response is the most prominent feature in the later periods of the simulations.

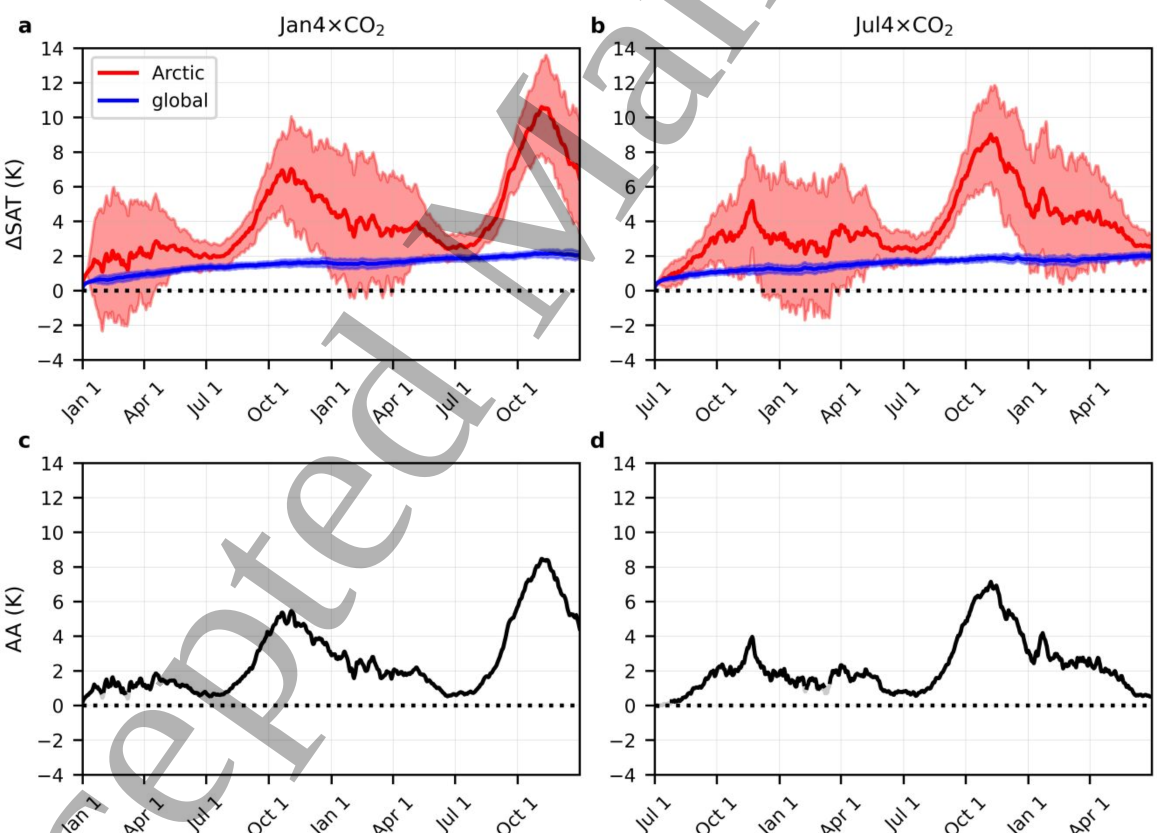

Fig. 1. (a,b) The average daily Arctic (70°N-90°N) and global change in SAT for the first two years of (a) Jan4×CO_2 and (b) Jul4×CO_2. Solid lines indicate the ensemble mean and the shading ±1 standard deviation. (c,d) Arctic amplification, defined as the difference in the ensemble mean Arctic and global average change in SAT for (c) Jan4×CO_2 and (d) Jul4×CO_2.

The line is opaque where the difference is significantly different from zero at the 95% confidence level.

To determine statistical significance, we perform a 1-sample Student's t-test on the time series of AA, shown in Fig. 1c & 1d. In the Jan4×CO_2, AA is statistically significant from day one and remains significant for almost the entire 2-year period, owing to the large ensemble size. In Jul4×CO_2, AA becomes consistently significant after 25 days and remains so, aside from 2 weeks in the first March. AA, therefore, can be detected well before the first three months following CO_2-quadrupling seen in Previdi et al. (2020), given sufficient ensemble size and temporal resolution. Until now, these ultrafast timescales of AA have been relatively unexplored in the existing body of AA research.

We note that the general features of the SAT and AA responses seen in Fig. 1 are robust to the number of ensemble members considered, although, not surprisingly, the responses are noisier and less statistically significant for smaller ensemble sizes (Fig. S1 & S2). The considerable noise in the Arctic SAT response (red lines) in Fig. S1a, S1c, & S1e and of Fig. S2a & S2c reflect the large internal variability present in the Arctic and the need for sufficiently large ensemble sizes in studies of Arctic climate.

Given the prominent role sea ice loss is thought to play in AA, we next explore how sea ice area (SIA) evolves over the same timescales. Sea ice loss is negligible in the first month of Jan4×CO_2 and remains relatively small through the rest of the winter and early spring (Fig. 2a, c), suggesting that sea ice loss plays a minimal role in AA on these short timescales. The decline in SIA accelerates through the late spring and summer, culminating in a ~30% decrease by the first September in Jan4×CO_2. The minimum in SIA precedes the seasonal AA maximum in Jan4×CO_2 by 1-2 months (Fig. 1c), implying a large role for sea ice loss in governing the seasonality of AA through its effects on ocean-atmosphere heat exchange (see additional discussion in Section 4.2).

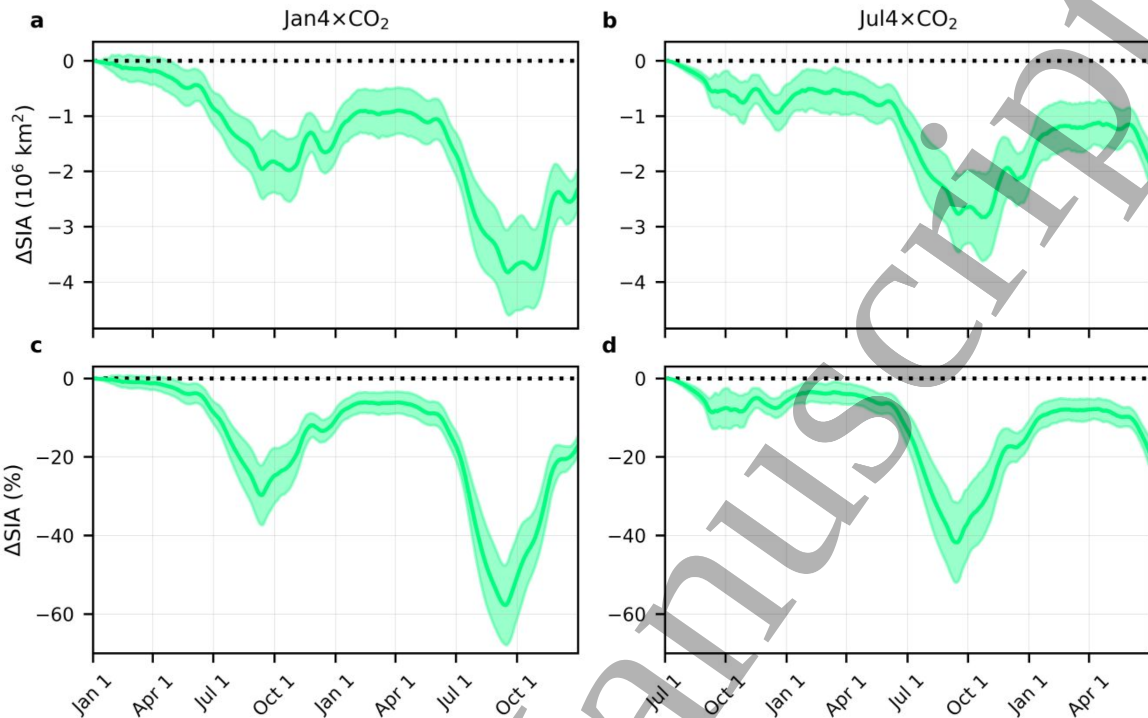

Fig. 2 (a,c) The daily average (a) absolute and (c) percent change in Arctic sea ice area (SIA) for the first two years of Jan4×CO_2. Solid lines indicate the ensemble mean and the shading ±1 standard deviation. (b, d) As in (a, c), but for Jul4×CO_2.

Sea ice loss exhibits a considerably different temporal structure in Jul4×CO_2 (Fig. 2b, d). We see a rapid decline in SIA over the first two months (~9% decrease by September), which then plateaus and slightly reverses through the following fall, winter, and spring. Interestingly, despite the immediate SIA reduction in Jul4×CO_2, AA is larger and more robust in the first month of Jan4×CO_2 with negligible sea ice loss. We discuss spatial changes in sea ice and their relationship with the surface air temperature response in Section 5.

4. Mechanism contributions to AA

4.1 Radiative Forcing

Having shown that AA becomes statistically significant almost immediately in Jan4×CO_2 and in the first month of Jul4×CO_2, we now quantify the time-varying warming contributions of different AA mechanisms. A natural place to start is the fundamental driver of the climate response, the radiative forcing (RF) associated with 4×CO_2 (Fig. 3). The magnitude of the 4×CO_2 RF at the TOA (Fig. 3a) is mainly determined by two factors: the climatological surface temperature and the temperature lapse rate. The climatological surface temperature governs the

RF via the Stefan-Boltzmann law: warmer surfaces produce more outgoing longwave radiation (OLR) for CO_2 to absorb and reemit into the atmospheric column (Raval & Ramanathan, 1989; Huang et al., 2016A). The lapse rate determines the temperature of the atmospheric layer from which OLR is effectively emitted to space; increased CO_2 can be thought of as increasing the height of this layer, or, equivalently, decreasing the effective emission temperature, making the lapse rate a pivotal factor in determining the TOA RF (Raval & Ramanathan, 1989; Huang et al., 2016A). The higher climatological surface temperature and larger temperature difference between the surface and upper troposphere in the global mean than in the Arctic yield a larger global mean TOA RF than Arctic mean TOA RF. Thus, when viewed from a TOA perspective, the CO_2 RF opposes AA.

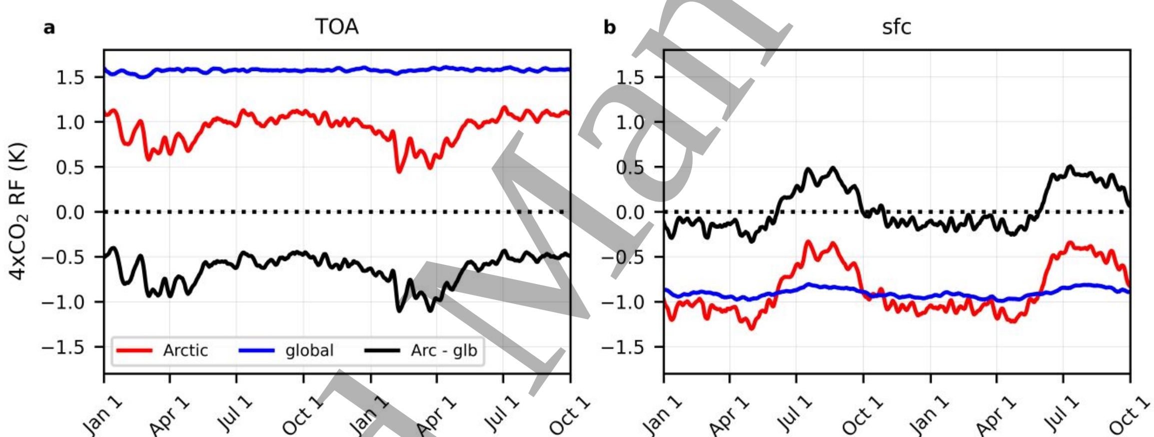

Fig. 3. The 7-day rolling average Arctic, global, and Arctic-global 4×CO_2 instantaneous radiative forcing from CESM-PORT at the (a) TOA and (b) surface, expressed as warming contributions to the global and Arctic average SAT responses. Positive values indicate energy entering the atmospheric column from the TOA or surface. See Section 2.3.2 for details on the conversion from radiative forcing (Wm^{-2}) to warming contributions (K).

A different story emerges when we consider the 4×CO_2 RF at the surface (Fig. 3b), which is strongly affected by the overlap in the spectral bands of CO_2 and water vapor (Kiehl & Ramanathan, 1982; Huang et al., 2017; Previdi et al., 2021). The forcing is consistently negative for both the Arctic and global average, indicating that the surface is gaining energy from the atmosphere. From October to April, the Arctic surface intercepts slightly more energy than the global average, opposing AA; this reverses in the summer.

Although we have treated the CO_2 RF as a standalone AA mechanism in the spirit of separating the forcing from the climate system response, we remind the reader that the surface CO_2 RF is incorporated into the surface heat uptake term (see Eq. 6). The contribution from the surface CO_2 RF to AA is small compared to the other terms in the surface energy budget that are discussed in section 4.3.

4.2 Atmospheric Column Energy Budget

Having examined the CO_2 forcing, we move on to feedbacks and energy transports from an atmospheric column perspective. We start by focusing exclusively on the first month following 4×CO_2 (Fig. 4). In Jan4×CO_2 (Fig. 4a), two mechanisms stand out as main AA contributors: the surface heat uptake (SHU), to be discussed in more detail later, and the lapse rate feedback. It is worth mentioning how the lapse rate feedback is thought to operate. Globally, the rate of temperature decrease with height in the troposphere is expected to decrease with increasing CO_2 – associated with enhanced warming at higher levels in the tropical troposphere – yielding a negative lapse rate feedback. In the Arctic, however, the climatologically stable temperature stratification of the lower troposphere traps warming near the surface and produces a positive lapse rate feedback (Graversen et al., 2014; Pithan & Mauritsen, 2014; Previdi et al., 2021). In the first month of Jan4×CO_2, the SHU and lapse rate feedback warm the Arctic up to 2.5K and 0.4K more than the global average, respectively, and are both statistically significant. Therefore, the rapid development of AA on short timescales in Jan4×CO_2 appears mainly to be a result of these two mechanisms. Previdi et al. (2020) found that the lapse rate feedback is a primary mechanism of AA on short timescales, and our results here support this. Other notable features in Fig. 4a are the Planck feedback that significantly contributes to AA only for the first few weeks and the cloud feedback that opposes AA throughout the first month in our model.

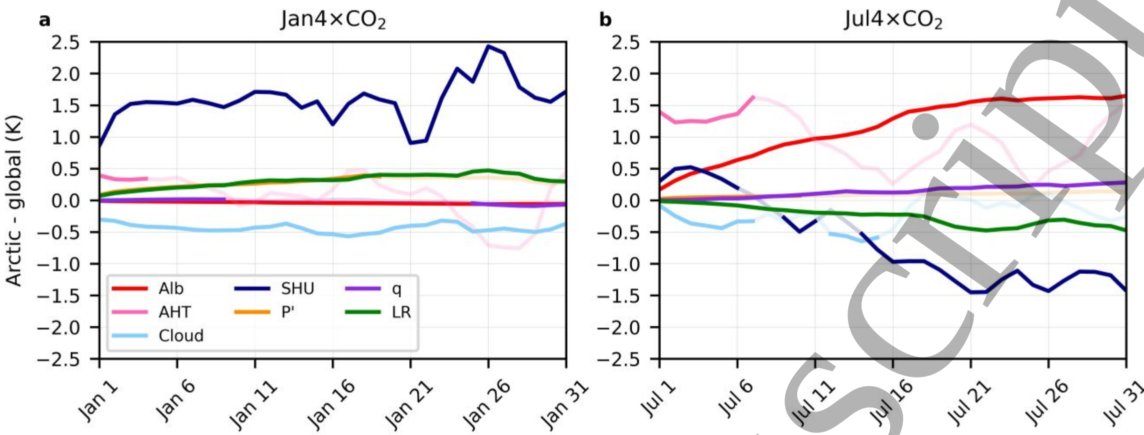

Fig. 4. The difference in Arctic and global average atmospheric column energy budget term responses for the first month of (a) Jan4×CO_2 and (b) Jul4×CO_2, expressed as warming contributions. These include the surface albedo feedback (Alb), atmospheric heat transport (AHT), cloud feedback (Cloud), surface heat uptake (SHU), local deviation of the Planck feedback (P'), water vapor feedback (q) and lapse rate feedback (LR) in the first month. Opaque lines indicate that the difference in Arctic and global warming contributions are significantly different from zero at the 95% level.

For Jul4×CO_2 (Fig. 4b), we find an initially positive AA contribution from SHU, but it becomes negligible and reverses (to oppose AA) within the first week. Instead, the AHT is the leading AA mechanism for the first week before becoming statistically nonsignificant and being surpassed by the surface albedo feedback. The surface albedo feedback remains the dominant AA-producing mechanism for the first month and is related to the rapid decline in sea ice seen in Fig. 2b & 2d and reductions in snow cover. Additionally, the water vapor feedback contributes to AA, albeit weakly.

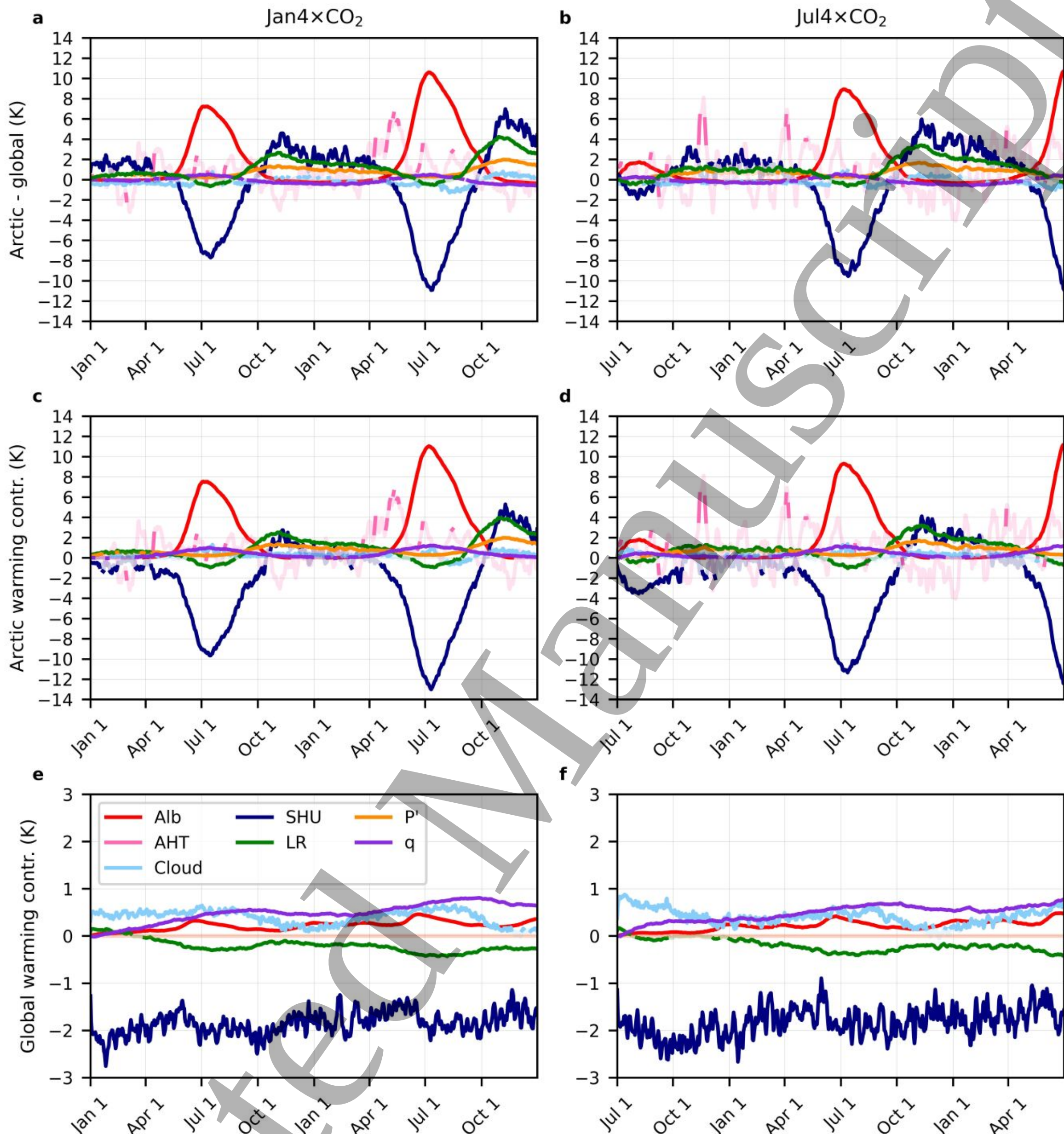

Fig. 5. (a, c, e) The (a) difference in Arctic and global average, (c) Arctic average, and (e) global average atmospheric column energy budget term responses in Jan4×CO_2, expressed as warming contributions. Opaque lines indicate where the contribution is statistically significant at the 95% level. (b, d, f) As in (a, c, e) but for Jul4×CO_2.

On timescales beyond the first month, other mechanisms become important in shaping the magnitude and seasonality of AA. As seen in Fig. 5a & b, the most striking features of the time-varying warming contributions to AA for both Jan4×CO_2 and Jul4×CO_2 (Fig. 5a & 5b) are the opposing peaks in the surface albedo feedback and SHU in boreal summer. The surface albedo feedback has typically been thought to be a major player in AA (Holland & Bitz, 2003; Winton, 2006; Bintanja & van der Linden, 2013; Dai, 2021); however, its seasonality does not match the seasonality of AA (see Fig. 1c & 1d), suggesting that other mechanisms must act to delay or modify its impacts. The opposing peaks in the surface albedo feedback and SHU in the summer supports the idea that as sea ice melts, incoming solar radiation that would otherwise have been reflected out to space is absorbed by the ocean surface. This additional heat absorbed by the ocean mixed layer is subsequently released to the atmosphere in fall and winter (e.g., Stroeve et al., 2012, Boeke & Taylor, 2018; Chung et al., 2021; Hahn et al., 2021; Jenkins & Dai, 2022), thus contributing to the peak in AA in these seasons.

A few of the other terms In Fig. 5 are worth mentioning, notably the Planck feedback. The Planck feedback reflects a change in outgoing longwave radiation in response to a given change in surface temperature, and its difference between the Arctic and global average is thought to be an important contributor to AA (Winton, 2006; Pithan & Mauritsen, 2014; Zhang et al., 2018; Henry & Merlis, 2019; Previdi et al., 2020). Although the Planck feedback produces a small but statistically significant contribution to AA beginning in the first March of Jan4×CO_2 (Fig. 5a), only in the following winter does it become one of the main AA-producing mechanisms. The water vapor feedback also makes small contributions to AA in boreal summer in both Jan4×CO_2 and Jul4×CO_2 (Fig. 5a & 5b). The water vapor feedback's peak contribution in the summer may be related to increased moisture transport into the Arctic, discussed later. Lastly, the atmospheric heat transport (AHT) is very noisy compared to the other terms and does not contribute robustly to AA (Fig. 5a & 5b).

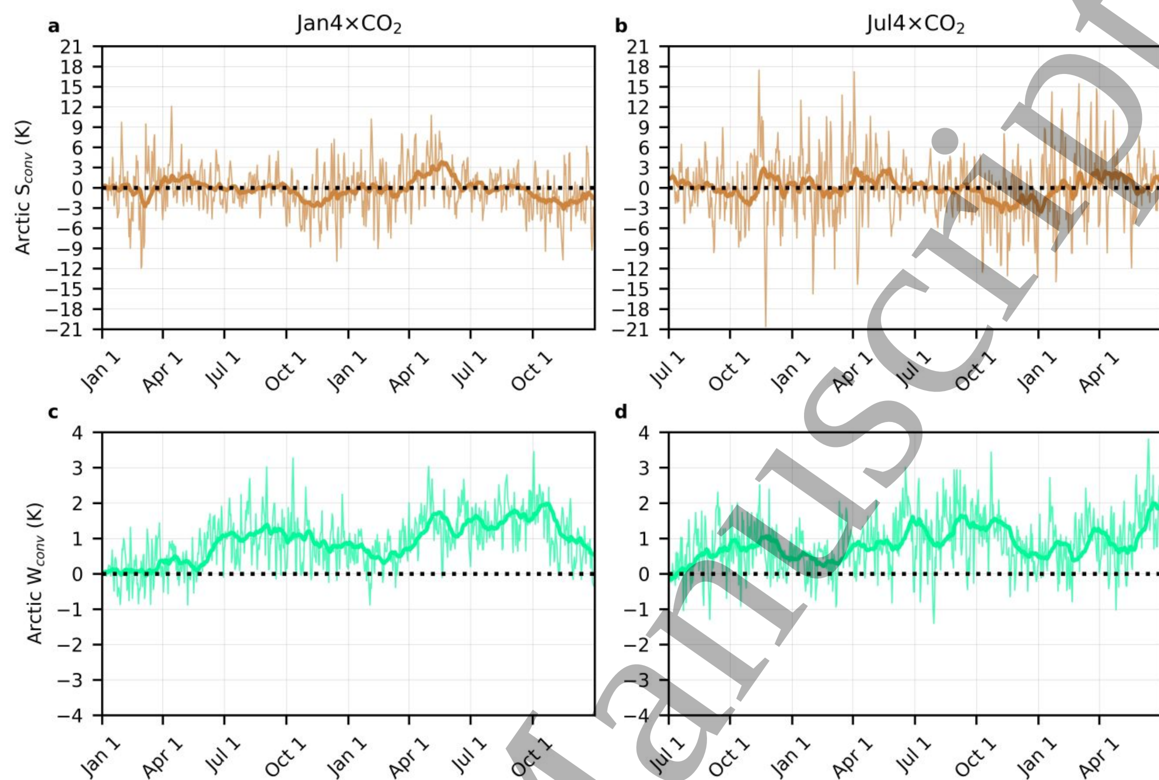

Fig. 6. (a,b) Arctic warming contributions by the dry static energy convergence (S_{conv}) for (a) Jan4×CO_2 (b) Jul4×CO_2. The ensemble means and 30-day rolling average ensemble means are denoted by thin and thick lines, respectively. (c,d) As in (a,b), but for the moisture flux convergence (W_{conv}). Note the difference in y-axis scales.

Let us now investigate further into this statistically nonsignificant AHT. Despite the lack of discernable signal in the total AHT, it is possible that the dry static energy convergence (S_{conv}) and the moisture flux convergence (W_{conv}) into the Arctic, shown in Fig. 6, individually contribute to the development of AA (Held & Soden, 2006). AA is generally associated with decreases in S_{conv} into the Arctic, resulting from the reduced latitudinal temperature gradient, and increases in W_{conv} into the Arctic, a product of the strengthening latitudinal specific humidity gradient (Hwang et al., 2011; Graversen & Burtu, 2016; Previdi et al., 2021). In particular, W_{conv} has been suggested to be a main driver of AA in the context of simplified models (Russotto & Biasutti, 2020). As we can see in Fig. 6, over the two years of our model simulations, S_{conv} is as noisy as the total AHT and does not consistently contribute to or oppose AA in either Jan4×CO_2 and Jul4×CO_2 (Fig. 6a & 6b). W_{conv} contributes to AA mainly during boreal summer (Fig. 6c & 6d); this coincides with periods of positive contributions to AA from the water vapor feedback seen in Fig. 5a & 5b. This suggests that W_{conv} affects the Arctic atmospheric energy budget both directly, and indirectly via the water vapor feedback (Gong et al., 2017; Russotto & Biasutti, 2020; Previdi et al., 2021). However, we stress that the development of AA in Jan4×CO_2 precedes any increase in the poleward moisture flux into the Arctic, meaning that the latter cannot explain the ultrafast development of AA following CO_2 increase.

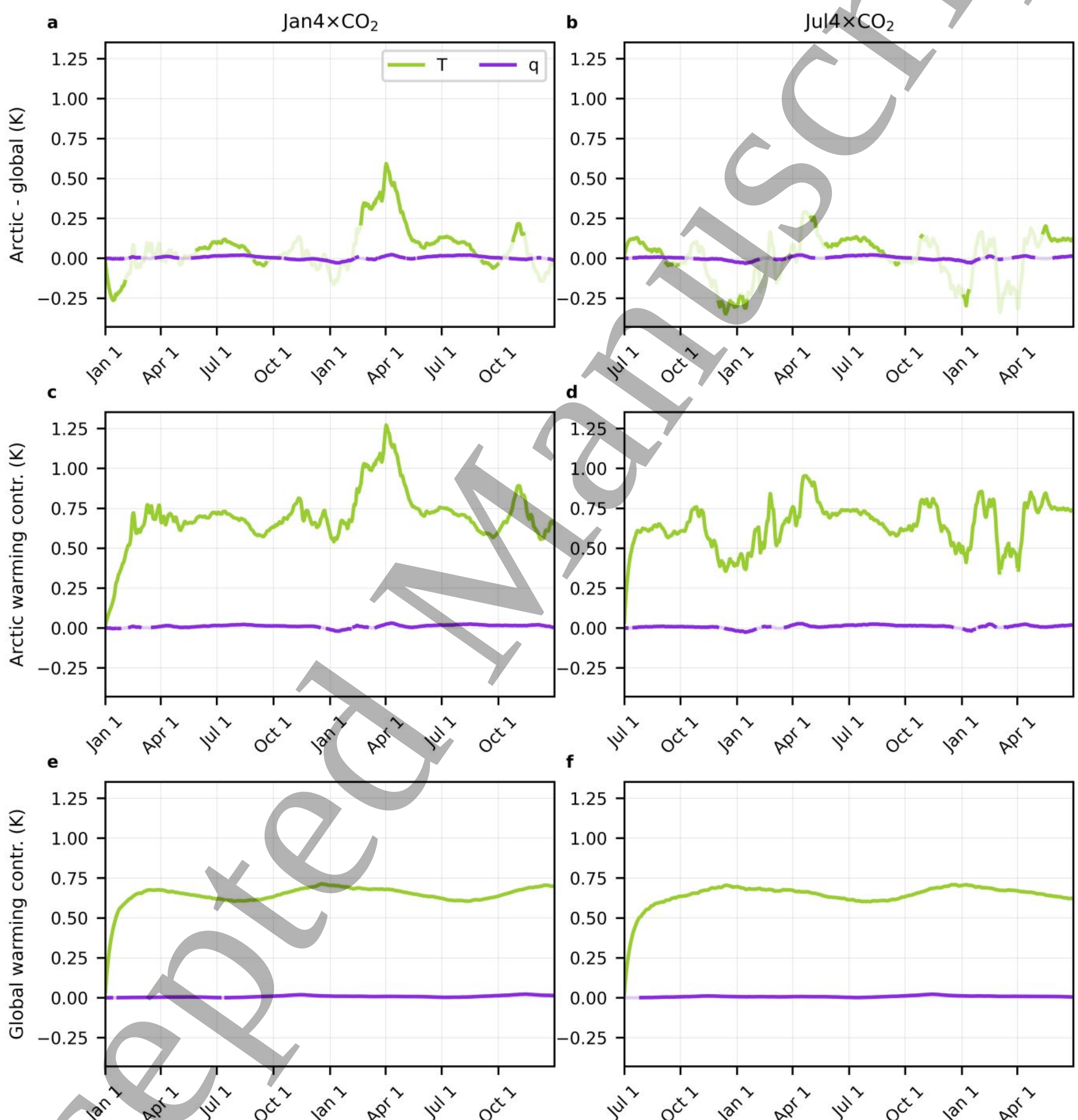

Fig. 7. As in Fig. 5, but for the stratospheric temperature and water vapor feedbacks.

Thus far in this section, we have considered only the tropospheric temperature and water vapor feedbacks. However, some studies have found that stratospheric feedbacks may play some role in the surface temperature response to increased CO_2 levels (Huang et al., 2016B; Banerjee et al., 2019). We have quantified the total temperature and water vapor feedbacks in the stratosphere (Fig. 7) and find that both are generally small contributions to AA compared to tropospheric feedbacks, aside from a brief period in the second spring of Jan4×CO_2 in which the stratospheric temperature feedback contributes up to ~0.55 K to AA in the ensemble mean.

4.3 Surface Energy Budget

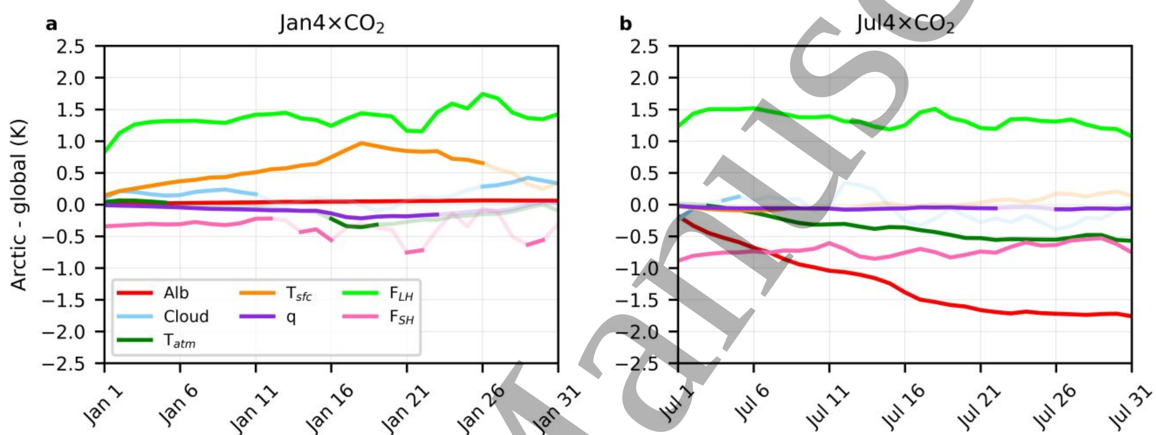

Fig. 8. The difference in Arctic and global average surface energy budget term responses for the first month of (a) Jan4×CO_2 and (b) Jul4×CO_2, expressed as warming contributions. These include the surface albedo feedback (Alb), cloud feedback (Cloud), atmospheric temperature feedback (T_{atm}), surface temperature feedback (T_{sfc}), water vapor feedback (q), latent heat flux (F_{LH}), and sensible heat flux (F_{SH}). Opaque lines indicate statistical significance at the 95% level. The sign convention is such that positive values correspond to upward (sea-to-air) fluxes.

The bulk of our analysis so far has focused on the atmospheric column energy budget from a TOA perspective. Given the leading role of SHU in Jan4×CO_2 in AA development (Fig. 4a) and the climatological stratification of the Arctic lower troposphere, we now take a closer look at the surface energy budget. We decompose the SHU response into contributions from radiative and non-radiative flux changes, which we show for the first month in Fig. 8, except for the CO_2 RF previously discussed in Section 4.1. One of the more conspicuous features of the time-varying surface energy balance is the strong positive contribution to AA by the latent heat flux (F_{LH}) in both Jan4×CO_2 and Jul4×CO_2 (Fig. 8a & 8b). Over the first few days, F_{LH} cools the global average ~1K and ~1.4K more than the Arctic in Jan4×CO_2 and Jul4×CO_2 respectively. The latent heat flux persists as the dominant AA mechanism at the surface for the remainder of the first month. In Jan4×CO_2, AA is further reinforced by the surface temperature feedback (Fig. 8a). In

450 Jul4×CO_2, AA is opposed by negative contributions from the sensible heat flux (F_{SH}) and the
451 surface albedo feedback (Fig. 8b). The magnitudes of other positive contribution terms are
452 smaller than F_{LH} in the first month, supporting the latent heat flux's leading role at the surface in
453 producing ultrafast development of AA.

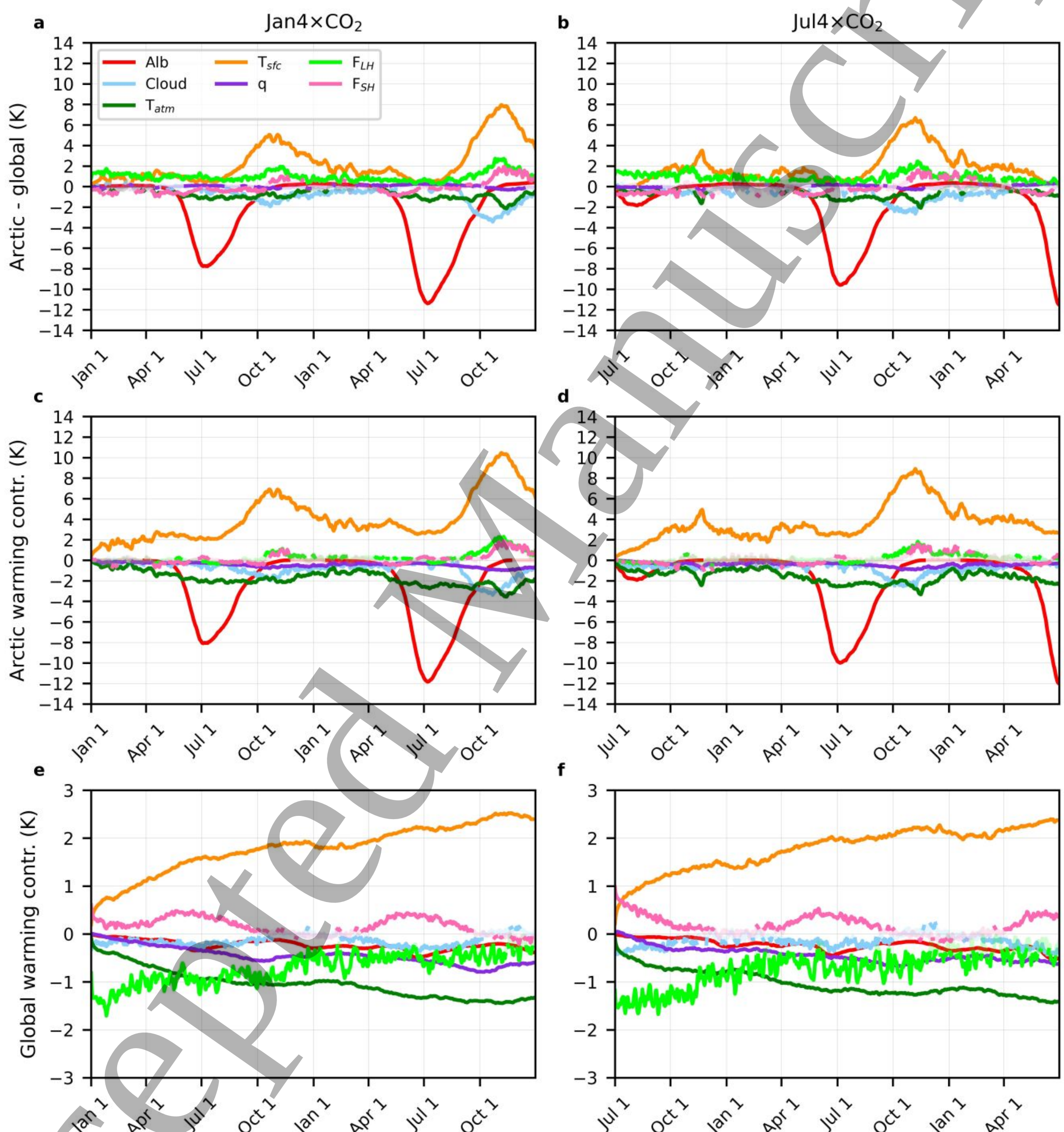

454

455 Fig. 9. The (a) difference in Arctic and global average, (c) Arctic average, and (e) global
456 average surface energy budget term responses in Jan4×CO_2, expressed as warming contributions.
457 Opaque lines indicate where the contribution is statistically significant at the 95% level. (b, d, f)
458 As in (a, c, e) but for Jul4×CO_2.
459

To determine if the latent heat flux stays the dominant term over longer timescales, we show the surface energy budget terms over the entire 2-year period in Fig. 9. The latent heat flux remains the largest positive contribution to AA in both Jan4×CO_2 and Jul4×CO_2, although the surface temperature feedback regularly surpasses it in the fall and winter as AA nears its peak (Fig. 9a & 9b); the strong positive surface temperature feedback in the Arctic (Fig. 9c & 9d) during these times reflects the large Arctic surface warming and associated enhancement of the surface upwelling LW radiation, a greater enhancement than occurs in the global average (Fig. 9e & 9f). Another prominent feature of the surface energy budget response is the recurring negative peaks in the surface albedo feedback in terms of both AA (Fig. 9a & 9b) and Arctic warming contributions (Fig. 9c & 9d). As previously stated, atmospheric warming from the surface albedo feedback in summer is not realized in that season, as the additional heat is absorbed by the ocean, producing these local minima in albedo warming contributions. Consistent with Boeke & Taylor (2018), small cold-season peaks in sensible and latent heat flux contributions to AA can be seen in Jan4×CO_2 and in the second year of Jul4×CO_2 as the energy stored in the ocean is released into the atmosphere.

The warming contribution of the surface latent heat flux to AA on short timescales (Fig. 8 & Fig. 9a & 9b) warrants further discussion. It is well-established that rapid adjustments of the global hydrological cycle occur following a perturbation in atmospheric CO_2. Specifically, because of the difference in CO_2 radiative forcing at the TOA and surface (Fig. 3), atmospheric radiative cooling decreases as CO_2 increases. This decrease in atmospheric radiative cooling must be balanced in the global mean by a decrease in latent heating from precipitation, and thus a decrease in the upward surface latent heat flux (Allen & Ingram, 2002; Bala et al., 2010). This is reflected in the strong negative global F_{LH} anomaly occurring immediately after 4×CO_2 in both Jan4×CO_2 and Jul4×CO_2 (Fig. 9e & 9f). Over the Arctic, any fast response of the surface F_{LH} is much smaller (Fig. 9c & 9d), resulting in a strong positive contribution from this term to AA.

5. Arctic land vs. ocean response

Given the prominent role of SHU in AA development in Jan4×CO_2 and the potential role of sea ice, it is useful to consider the responses over Arctic land and ocean areas separately. We choose a few timescales over which to summarize the development of AA: the first month, the

489 first three months, and the first year after $4\times CO_2$. The first month roughly corresponds to the earliest timeframe in which AA is statistically significant in both the January- and July-initialized simulations, the first three months correspond to the earliest timescale analyzed in Previdi et al. (2020), and the first year captures the first complete annual cycle following $4\times CO_2$.

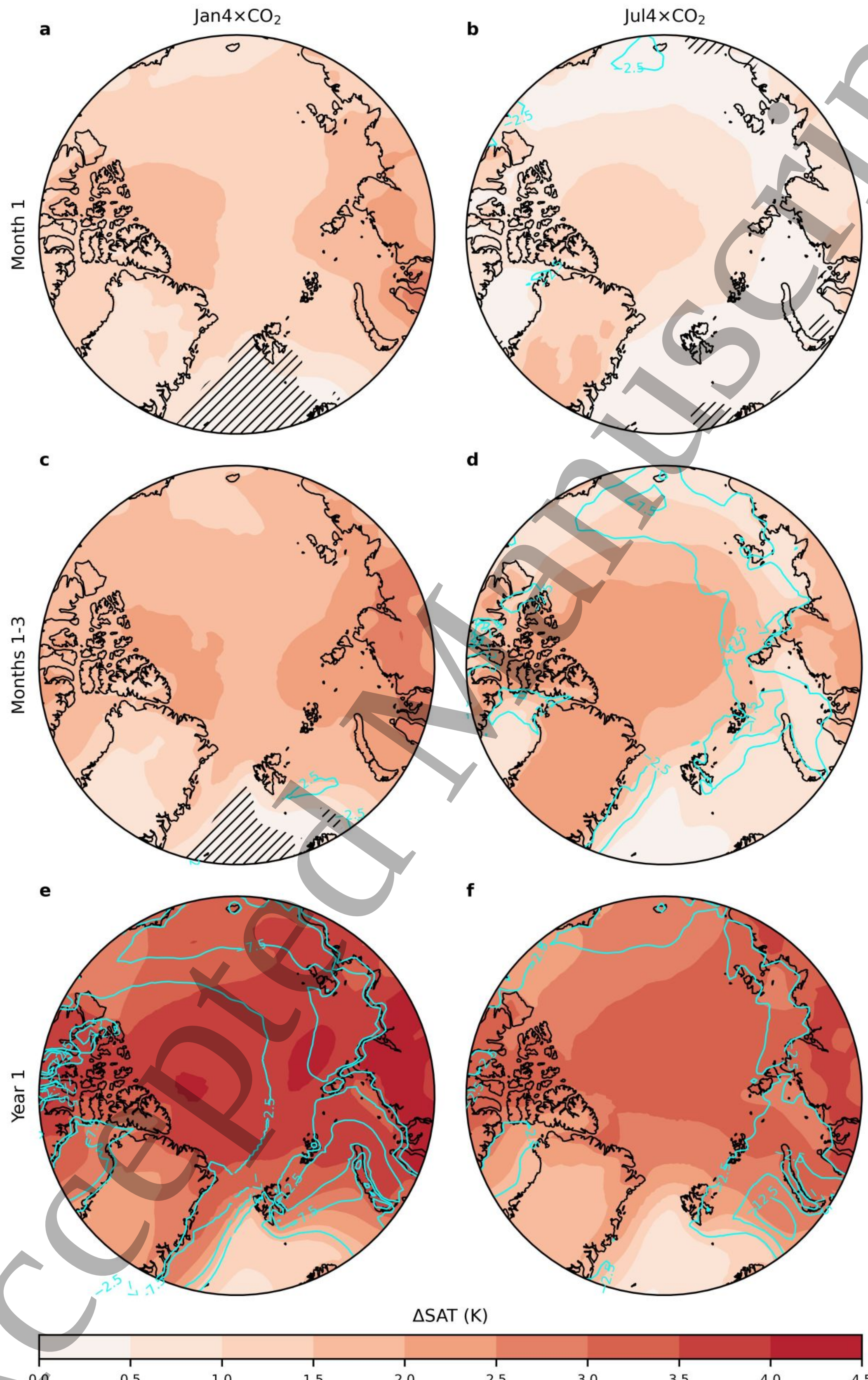
Jan4×CO2
Jul4×CO2
a
b
c
d
e
f
Month 1
Months 1-3
Year 1
ΔSAT (K)
0.0
0.5
1.0
1.5
2.0
2.5
3.0
3.5
4.0
4.5

493

Fig. 10. (a,c,e) The change in SAT (shading) and sea ice concentration (aqua contours, %) averaged over the (a) first month, (c) first three months, and (e) first year following $4\times CO_2$ in CESM-LE members initialized January. Hatching indicates areas where the SAT response is not statistically significant at the 95% confidence level. (b,d,e) As in (a,c,e), but for July.

The spatial distribution of warming, and its relationship to changes in Arctic sea ice, for these periods is shown in Fig. 10. In the first month of Jan4$\times CO_2$, there is statistically significant warming over the entire Arctic domain except the Nordic Seas, with a local maximum in northern Siberia (Fig. 10a). Warming strengthens and spreads to include the entire domain over the first three months (Fig. 10c) and first year (Fig. 10e). Although Jul4$\times CO_2$ exhibits a greater decrease in sea ice in the first few months, the warming signal appears to be amplified over land rather than the ocean (Fig. 10b & 10d). By the end of the first year, Jan4$\times CO_2$ and Jul4$\times CO_2$ show similar spatial warming patterns, although overall warming is greater in Jan4$\times CO_2$ (Fig. 10e & 10f). By comparing the spatial distribution of SAT and SIC response on all three timescales, it is apparent that areas of maximum warming are *not* co-located with areas of maximum sea ice loss. This key result further demonstrates that mechanisms other than sea ice loss dominate the surface temperature response at these short timescales; however, we note that in the summer sea ice melt season (Fig. 10b & 10d), Arctic SSTs are constrained to remain near the freezing point; thus, we expect greater warming over land where there is no such constraint.

To test the presence of land- or ocean-amplified warming, we show a time series of the SAT response averaged over Arctic land and ocean separately (Fig. S3). In both Jan4$\times CO_2$ (Fig. S3a & S3c) and Jul4$\times CO_2$ (Fig. S3b & S3d), a seasonal cycle emerges consisting of land-amplified warming in the summer and ocean-amplified warming in the fall and winter. Fig. S3d confirms our suspicion from Fig. 10b & 10d that there is statistically significant land-amplified warming over the first few months of Jul4$\times CO_2$.

To better understand the land and ocean SAT responses, we have calculated the warming contributions to the Arctic atmospheric column from a TOA perspective for the three time periods, for the land and ocean separately (Fig. 11). As one might expect, SHU is the term with the largest land-ocean difference over all periods in both Jan4$\times CO_2$ and Jul4$\times CO_2$, with the ensemble mean SHU response consistently at least three-times more negative over the ocean than over land. In Jan4$\times CO_2$, this tendency for SHU to preferentially warm land is compensated by temperature feedbacks and AHT in the first few months (Fig. 11a & 11c), yielding little difference in the Arctic land and ocean temperature responses. The SHU is partially, but not fully, compensated by the surface albedo feedback on short timescales in Jul4×CO_2, producing the land-amplified warming seen in Fig. S3b & S3d.

Given the magnitude of the SHU on short timescales relative to other terms in the TOA energy budget, we again decompose the SHU into individual terms in Fig. S4. As a reminder, the sign of the surface heat flux terms is chosen such that positive indicates the movement of energy from the surface to the atmospheric column. The sensible heat flux appears to be the main cause of land-over-ocean SHU warming in the first month and first three months of Jan4×CO_2 because it is positive over land and negative over the ocean (Fig. S4a & S4c). Over the first year of Jan4×CO_2 and all periods in Jul4×CO_2, the surface albedo feedback dominates land-over-ocean warming since it is considerably more negative for the ocean than land (Fig. S4b, S4d-f). In other words, the surface albedo feedback moves a greater amount of energy from the atmospheric column into the ocean than into land. Thus, the surface albedo feedback and sensible heat fluxes are the main drivers of the large contribution of SHU to the different Arctic land and ocean SAT responses.

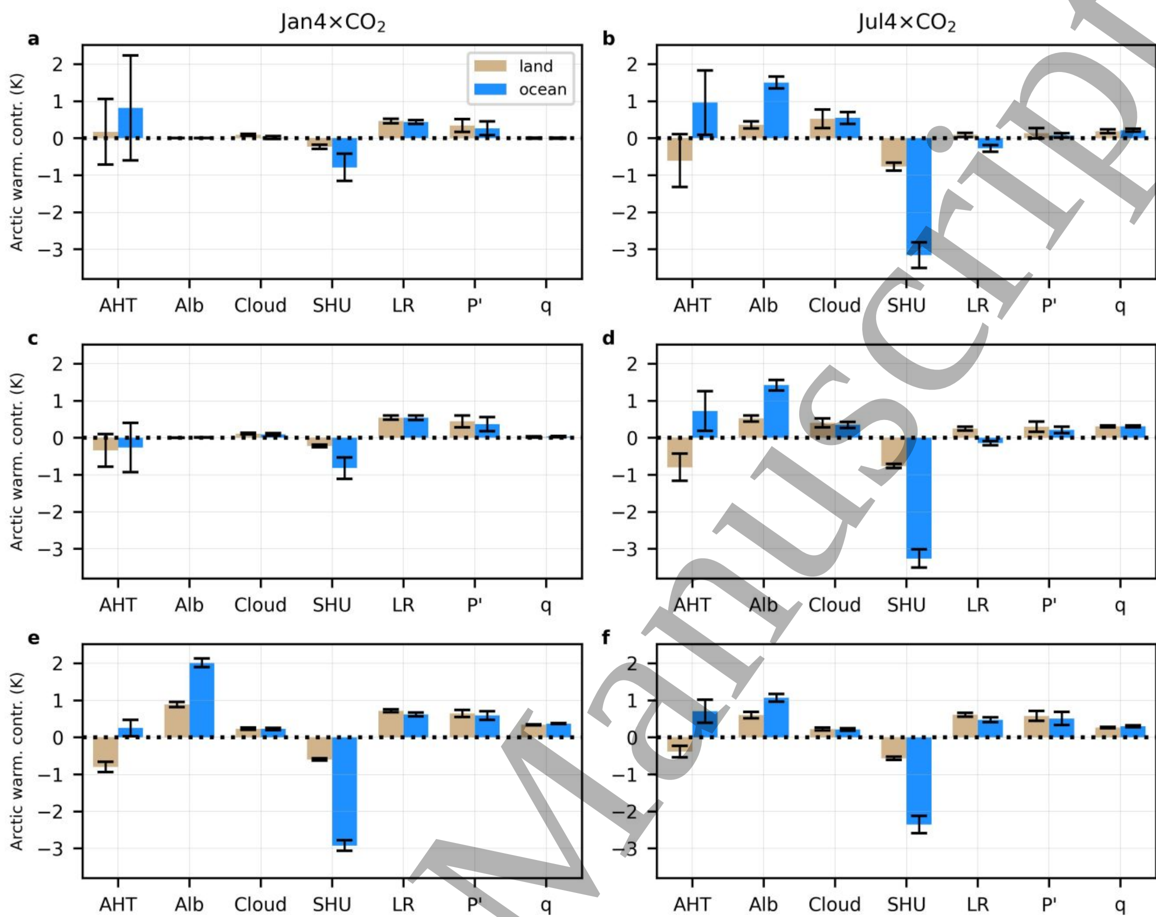

Fig. 11. (a, c, e) Atmospheric column energy budget terms from a TOA perspective averaged over the (a) first month, (c) first three months, and (e) first year of Jan4×CO_2. The error bars denote 95% confidence intervals. (b, d, f) As in (a, c, e), but for Jul4×CO_2.

6. Conclusions

In this study, we used two large ensembles of GCM simulations, one in which CO_2 is instantaneously quadrupled in January, the other in July, and observed how fast AA develops. We then attributed the AA response to local feedbacks and energy transports using an energy budget analysis from both TOA and surface perspectives. Finally, we analyzed the spatial pattern of Arctic warming and decomposed Arctic warming contributions into land and ocean components. Our results now allow us to revisit the key questions posed in the introduction:

How quickly does AA develop in an ensemble of model simulations subjected to an instantaneous CO_2 increase? Following a quadrupling of CO_2 in January or July, statistically significant AA develops in less than a month. In Jan4×CO_2, AA develops immediately (i.e., on day 1) after the radiative forcing is applied, whereas robust AA develops after 25 days in Jul4×CO_2.

To the best of our knowledge, our findings are novel in that AA has rarely been examined on such short timescales, with previous studies focusing on much longer (e.g., multi-decadal) timescales. An exception to this is the recent study by Previdi et al. (2020). In that study, which used monthly mean model output, AA was present after three months following an abrupt quadrupling of CO_2 in January. Our use of large ensembles of daily output for the present study allowed AA to be detected considerably earlier with the same CO_2 forcing. Notably, AA precedes any statistically significant decrease in Arctic sea ice in January-initialized simulations; conversely, AA development tends to lag the response of the sea ice area in Jul4×CO_2. This demonstrates that the development of AA does not require a decrease in Arctic sea ice, confirming the findings of Previdi et al. (2020) and supports the results of several other modeling studies that employed locked sea ice/surface albedo feedbacks (Graversen & Wang, 2009; Graversen et al., 2014, Merlis 2014, Dekker et al., 2019) and aquaplanets without sea ice (Langen & Alexeev, 2007; Langen et al., 2012; Russotto & Biasutti, 2020).

What mechanisms best explain the initial appearance and the subsequent evolution of AA? From an atmospheric column energy budget perspective, SHU and, to a lesser extent, the lapse rate feedback are the dominant mechanisms by which AA develops in Jan4×CO_2. A similar positive contribution from the lapse rate feedback on short timescales was also documented by Previdi et al. (2020). Jul4×CO_2 shows a similar initially positive contribution to AA from SHU, but it becomes negligible in the first week. Instead, in Jul4×CO_2, the surface albedo feedback appears to be the leading mechanism by which AA develops on short timescales.

Upon decomposing the SHU response, we found that the difference in the Arctic and global average surface latent heat flux response produces AA on ultrafast timescales. The difference in 4×CO_2 surface radiative forcing between the Arctic and global average further contributes to this ultrafast AA response in Jul4×CO_2 but is much smaller. The rapid response of the surface latent heat flux that we have documented here, which is dominated by a strong reduction in the global-mean surface evaporation, has previously been recognized as a rapid adjustment to increasing atmospheric CO_2 in studies of the global hydrological cycle (Allen &

Ingram, 2002; Bala et al., 2010). However, it is our understanding that this study is the first to recognize its importance for AA.

On longer timescales (i.e., > 1 month), other mechanisms become important in shaping the evolution of AA in the simulations. The most prominent contribution to AA in both Jan4×CO_2 and Jul4×CO_2 comes from the summertime surface albedo feedback; increased moisture flux convergence and water vapor feedback are additional smaller contributions to AA in the summer. Despite this, AA is absent (or very weak) during the summer months, which can be explained by the substantially negative SHU contribution and, to a lesser extent, the lapse rate feedback. The strongly negative SHU contribution reflects the absorption of excess heat by the ocean mixed layer (mainly due to the surface albedo feedback). This excess heat is released into the atmosphere later in the year. By autumn, AA begins to strengthen and reaches its peak intensity at the end of October, with positive contributions from the Planck feedback, lapse rate feedback, and SHU (Rigor et al., 2002; Serreze et al., 2009; Screen & Simmonds, 2010; Stroeve et al., 2012; Boeke & Taylor, 2018; Chung et al., 2021; Hahn et al., 2021; Jenkins & Dai, 2022).

We stress that commonly cited AA mechanisms like sea ice loss and the moisture flux convergence into the Arctic are not unimportant, but rather cannot explain the ultrafast development of AA after CO_2 increase. Our results show that the leading causes of AA depend on the timescale examined, a nuance often overlooked in the existing body of AA research. Although an abrupt quadrupling of CO_2 is a highly idealized radiative forcing chosen for the purpose of this study, the evolutions of feedbacks and energy transports are likely important considerations for any study of AA mechanisms.

How does the time of year in which atmospheric CO_2 is quadrupled affect AA development? AA is slower to develop in Jul4×CO_2 than in Jan4×CO_2 (25 days vs. one day), hampered by an immediately negative Arctic lapse rate feedback and a negative contribution from SHU. This result is unsurprising, given the well-known summertime minimum in AA (Laîné et al., 2016; Previdi et al., 2021). Despite this, robust AA forms by the end of the first month in both experiments and persists through most of the following two years. Maximum Arctic SAT increase in Jan4×CO_2 and Jul4×CO_2 occurs over land areas, further evidence that sea ice loss is not the dominant mechanism in the rapid development of AA.

It is interesting to consider whether the ultrafast SHU and lapse rate responses documented here (i.e., those occurring in the first few days to weeks of 4×CO_2) may be classified as rapid adjustments, which are defined as the response to an external forcing that is independent of global surface temperature change (Forster et al., 2013). Given that the global SAT change is small on these fast timescales, the adjustment framework may be appropriate. To the extent that it is, it would suggest that AA fundamentally owes its existence to rapid adjustments, which act to enhance Arctic warming before slower components of the climate system, such as sea ice, have a chance to respond. The ultrafast response of the Arctic to radiative forcing implies the potential for significant near-term mitigation of Arctic warming if humanity acts quickly to reduce atmospheric CO_2.

7. Funding

TJ, MP, KS and LP were funded by the National Science Foundation Office of Polar Programs, Arctic Research Opportunities Grant # PLR-1603350. TJ was also funded by the National Science Foundation Graduate Research Fellowship Program, Grant # DGE-2036197. GC was funded by the National Swiss Science Foundation Ambizione Grant #PZ00P2_180043.

7. Acknowledgements

The authors gratefully acknowledge the NCAR Large Ensemble Community Project and supercomputing resources provided by the National Center for Atmospheric Research Computing and Informational Systems Lab, technical support from Dr. Gustavo Correa, and the insightful contributions from two anonymous reviewers.

8. Data availability statement

All code used in data analysis and visualization is publicly available at https://doi.org/10.5281/zenodo.7998734. The CESM simulations that support the findings of this study are available upon request from the authors.

References

Allen, M. R., & Ingram, W. J. (2002). Constraints on future changes in climate and the hydrologic cycle. *Nature*, *419*(6903), 228–232. https://doi.org/10.1038/nature01092

Altdorff, D., Borchard, N., Young, E. H., Galagedara, L., Sorvali, J., Quideau, S., & Unc, A. (2021). Agriculture in boreal and Arctic regions requires an integrated global approach for research and policy. *Agronomy for Sustainable Development*, *41*(2), 23. https://doi.org/10.1007/s13593-021-00676-1

Arrhenius, S. (1896). XXXI. On the influence of carbonic acid in the air upon the temperature of the ground. *The London, Edinburgh, and Dublin Philosophical Magazine and Journal of Science*, *41*(251), 237–276. https://doi.org/10.1080/14786449608620846

Bala, G., Caldeira, K., & Nemani, R. (2010). Fast versus slow response in climate change: implications for the global hydrological cycle. *Climate Dynamics*, *35*(2), 423–434. https://doi.org/10.1007/s00382-009-0583-y

Banerjee, A., Chiodo, G., Previdi, M., Ponater, M., Conley, A. J., & Polvani, L. M. (2019). Stratospheric water vapor: an important climate feedback. *Climate Dynamics*, *53*(3), 1697–1710. https://doi.org/10.1007/s00382-019-04721-4

Bintanja, R., & Krikken, F. (2016). Magnitude and pattern of Arctic warming governed by the seasonality of radiative forcing. *Scientific Reports*, *6*(1), 38287. https://doi.org/10.1038/srep38287

Bintanja, R., & van der Linden, E. C. (2013). The changing seasonal climate in the Arctic. *Scientific Reports*, *3*(1), 1556. https://doi.org/10.1038/srep01556

Bitz, C. M., Gent, P. R., Woodgate, R. A., Holland, M. M., & Lindsay, R. (2006). The Influence of Sea Ice on Ocean Heat Uptake in Response to Increasing CO2. *Journal of Climate*, *19*(11), 2437–2450. https://doi.org/10.1175/JCLI3756.1

Boeke, R. C., & Taylor, P. C. (2018). Seasonal energy exchange in sea ice retreat regions contributes to differences in projected Arctic warming. *Nature Communications*, *9*(1), 5017. https://doi.org/10.1038/s41467-018-07061-9

Boeke, R. C., Taylor, P. C., & Sejas, S. A. (2021). On the Nature of the Arctic's Positive Lapse-Rate Feedback. *Geophysical Research Letters*, *48*(1), e2020GL091109. https://doi.org/10.1029/2020GL091109

Cao, Y., Liang, S., Chen, X., He, T., Wang, D., & Cheng, X. (2017). Enhanced wintertime greenhouse effect reinforcing Arctic amplification and initial sea-ice melting. *Scientific Reports*, *7*(1), 8462. https://doi.org/10.1038/s41598-017-08545-2

Chung, E.-S., Ha, K.-J., Timmermann, A., Stuecker, M. F., Bodai, T., & Lee, S.-K. (2021). Cold-Season Arctic Amplification Driven by Arctic Ocean-Mediated Seasonal Energy Transfer. *Earth's Future*, *9*(2), e2020EF001898. https://doi.org/10.1029/2020EF001898

Cohen, J., Screen, J. A., Furtado, J. C., Barlow, M., Whittleston, D., Coumou, D., et al. (2014). Recent Arctic amplification and extreme mid-latitude weather. *Nature Geoscience*, *7*(9), 627–637. https://doi.org/10.1038/ngeo2234

Conley, A. J., Lamarque, J.-F., Vitt, F., Collins, W. D., & Kiehl, J. (2013). PORT, a CESM tool for the diagnosis of radiative forcing. *Geoscientific Model Development*, *6*(2), 469–476. https://doi.org/10.5194/gmd-6-469-2013

Crook, J. A., Forster, P. M., & Stuber, N. (2011). Spatial Patterns of Modeled Climate Feedback and Contributions to Temperature Response and Polar Amplification. *Journal of Climate*, *24*(14), 3575–3592. https://doi.org/10.1175/2011JCLI3863.1

Dai, H. (2021). Roles of Surface Albedo, Surface Temperature and Carbon Dioxide in the Seasonal Variation of Arctic Amplification. *Geophysical Research Letters*, *48*(4), e2020GL090301. https://doi.org/10.1029/2020GL090301

Dekker, E., Bintanja, R., & Severijns, C. (2019). Nudging the Arctic Ocean to Quantify Sea Ice Feedbacks. *Journal of Climate*, *32*(8), 2381–2395. https://doi.org/10.1175/JCLI-D-18-0321.1

England, M., Jahn, A., & Polvani, L. (2019). Nonuniform Contribution of Internal Variability to Recent Arctic Sea Ice Loss. *Journal of Climate*, *32*(13), 4039–4053. https://doi.org/10.1175/JCLI-D-18-0864.1

Feldl, N., Bordoni, S., & Merlis, T. M. (2017). Coupled High-Latitude Climate Feedbacks and Their Impact on Atmospheric Heat Transport. *Journal of Climate*, *30*(1), 189–201. https://doi.org/10.1175/JCLI-D-16-0324.1

Feldl, N., Po-Chedley, S., Singh, H. K. A., Hay, S., & Kushner, P. J. (2020). Sea ice and atmospheric circulation shape the high-latitude lapse rate feedback. *Npj Climate and Atmospheric Science*, *3*(1), 1–9. https://doi.org/10.1038/s41612-020-00146-7

Feldl, N., & Roe, G. H. (2013). Four perspectives on climate feedbacks. *Geophysical Research Letters*, *40*(15), 4007–4011. https://doi.org/10.1002/grl.50711

Forster, P. M., Andrews, T., Good, P., Gregory, J. M., Jackson, L. S., & Zelinka, M. (2013). Evaluating adjusted forcing and model spread for historical and future scenarios in the CMIP5 generation of climate models. *Journal of Geophysical Research: Atmospheres*, *118*(3), 1139–1150. https://doi.org/10.1002/jgrd.50174

Francis, J. A., & Vavrus, S. J. (2012). Evidence linking Arctic amplification to extreme weather in mid-latitudes. *Geophysical Research Letters*, *39*(6). https://doi.org/10.1029/2012GL051000

Gong, T., Feldstein, S., & Lee, S. (2017). The Role of Downward Infrared Radiation in the Recent Arctic Winter Warming Trend. *Journal of Climate*, *30*(13), 4937–4949. https://doi.org/10.1175/JCLI-D-16-0180.1

Goosse, H., Kay, J. E., Armour, K. C., Bodas-Salcedo, A., Chepfer, H., Docquier, D., et al. (2018). Quantifying climate feedbacks in polar regions. *Nature Communications*, *9*(1), 1919. https://doi.org/10.1038/s41467-018-04173-0

Graversen, R. G., & Burtu, M. (2016). Arctic amplification enhanced by latent energy transport of atmospheric planetary waves. *Quarterly Journal of the Royal Meteorological Society*, *142*(698), 2046–2054. https://doi.org/10.1002/qj.2802

Graversen, R. G., & Langen, P. L. (2019). On the Role of the Atmospheric Energy Transport in 2 × CO2–Induced Polar Amplification in CESM1. *Journal of Climate*, *32*(13), 3941–3956. https://doi.org/10.1175/JCLI-D-18-0546.1

Graversen, R. G., Langen, P. L., & Mauritsen, T. (2014). Polar Amplification in CCSM4: Contributions from the Lapse Rate and Surface Albedo Feedbacks. *Journal of Climate*, *27*(12), 4433–4450. https://doi.org/10.1175/JCLI-D-13-00551.1

724 Graversen, R. G., & Wang, M. (2009). Polar amplification in a coupled climate model with locked albedo. *Climate Dynamics*, *33*(5), 629–643. https://doi.org/10.1007/s00382-009-0535-6

727 Hahn, L. C., Armour, K. C., Zelinka, M. D., Bitz, C. M., & Donohoe, A. (2021). Contributions to Polar Amplification in CMIP5 and CMIP6 Models. *Frontiers in Earth Science*, *9*(710036). https://doi.org/10.3389/feart.2021.710036

730 Held, I. M., & Soden, B. J. (2006). Robust Responses of the Hydrological Cycle to Global Warming. *Journal of Climate*, *19*(21), 5686–5699. https://doi.org/10.1175/JCLI3990.1

732 Ho, J. (2010). The implications of Arctic sea ice decline on shipping. *Marine Policy*, *34*(3), 713–715. https://doi.org/10.1016/j.marpol.2009.10.009

734 Holland, M. M., & Bitz, C. M. (2003). Polar amplification of climate change in coupled models. *Climate Dynamics*, *21*(3), 221–232. https://doi.org/10.1007/s00382-003-0332-6

736 Huang, Y., Tan, X., & Xia, Y. (2016). Inhomogeneous radiative forcing of homogeneous greenhouse gases. *Journal of Geophysical Research: Atmospheres*, *121*(6), 2780–2789. https://doi.org/10.1002/2015JD024569

739 Huang, Y., Xia, Y., & Tan, X. (2017). On the pattern of CO2 radiative forcing and poleward energy transport. *Journal of Geophysical Research: Atmospheres*, *122*(20), 10,578-10,593. https://doi.org/10.1002/2017JD027221

742 Huang, Y., Zhang, M., Xia, Y., Hu, Y., & Son, S.-W. (2016). Is there a stratospheric radiative feedback in global warming simulations? *Climate Dynamics*, *46*(1), 177–186. https://doi.org/10.1007/s00382-015-2577-2

745 Hurrell, J. W., Holland, M. M., Gent, P. R., Ghan, S., Kay, J. E., Kushner, P. J., et al. (2013). The Community Earth System Model: A Framework for Collaborative Research. *Bulletin of the American Meteorological Society*, *94*(9), 1339–1360. https://doi.org/10.1175/BAMS-D-12-00121.1

749 Hwang, Y.-T., Frierson, D. M. W., & Kay, J. E. (2011). Coupling between Arctic feedbacks and changes in poleward energy transport. *Geophysical Research Letters*, *38*(17). https://doi.org/10.1029/2011GL048546

Jahn, A., Kay, J. E., Holland, M. M., & Hall, D. M. (2016). How predictable is the timing of a summer ice-free Arctic? *Geophysical Research Letters*, *43*(17), 9113–9120. https://doi.org/10.1002/2016GL070067

Jenkins, M. T., & Dai, A. (2022). Arctic Climate Feedbacks in ERA5 Reanalysis: Seasonal and Spatial Variations and the Impact of Sea-Ice Loss. *Geophysical Research Letters*, *49*(16), e2022GL099263. https://doi.org/10.1029/2022GL099263

Kay, J. E., Deser, C., Phillips, A., Mai, A., Hannay, C., Strand, G., et al. (2015). The Community Earth System Model (CESM) Large Ensemble Project: A Community Resource for Studying Climate Change in the Presence of Internal Climate Variability. *Bulletin of the American Meteorological Society*, *96*(8), 1333–1349. https://doi.org/10.1175/BAMS-D-13-00255.1

Kay, J. E., & Deser, C. (2016). The Community Earth System Model (CESM) Large Ensemble Project. *UCAR/NCAR Climate Data Gateway*. https://doi.org/10.5065/d6j101d1

Kiehl, J. T., & Ramanathan, V. (1982). Radiative Heating Due to Increased CO2: The Role of H2O Continuum Absorption in the 12–18 μm Region. *Journal of the Atmospheric Sciences*, *39*(12), 2923–2926. https://doi.org/10.1175/1520-0469(1982)039<2923:RHDTIC>2.0.CO;2

Labe, Z., Magnusdottir, G., & Stern, H. (2018). Variability of Arctic Sea Ice Thickness Using PIOMAS and the CESM Large Ensemble. *Journal of Climate*, *31*(8), 3233–3247. https://doi.org/10.1175/JCLI-D-17-0436.1

Laîné, A., Yoshimori, M., & Abe-Ouchi, A. (2016). Surface Arctic Amplification Factors in CMIP5 Models: Land and Oceanic Surfaces and Seasonality. *Journal of Climate*, *29*(9), 3297–3316. https://doi.org/10.1175/JCLI-D-15-0497.1

Langen, P. L., & Alexeev, V. A. (2007). Polar amplification as a preferred response in an idealized aquaplanet GCM. *Climate Dynamics*, *29*(2), 305–317. https://doi.org/10.1007/s00382-006-0221-x

Langen, P. L., Graversen, R. G., & Mauritsen, T. (2012). Separation of Contributions from Radiative Feedbacks to Polar Amplification on an Aquaplanet. *Journal of Climate*, *25*(8), 3010–3024. https://doi.org/10.1175/JCLI-D-11-00246.1

Lee, S. (2014). A theory for polar amplification from a general circulation perspective. *Asia-Pacific Journal of Atmospheric Sciences*, *50*(1), 31–43. https://doi.org/10.1007/s13143-014-0024-7

van der Linden, E. C., Le Bars, D., Bintanja, R., & Hazeleger, W. (2019). Oceanic heat transport into the Arctic under high and low CO_2 forcing. *Climate Dynamics*, *53*(7), 4763–4780. https://doi.org/10.1007/s00382-019-04824-y

Manabe, S., & Stouffer, R. J. (1980). Sensitivity of a global climate model to an increase of CO2 concentration in the atmosphere. *Journal of Geophysical Research: Oceans*, *85*(C10), 5529–5554. https://doi.org/10.1029/JC085iC10p05529

Meltofte, H., Barry, T., Berteaux, D., Bültmann, H., Christiansen, J. S., Cook, J. A., et al. (2013). *Arctic Biodiversity Assessment. Synthesis.* Conservation of Arctic Flora and Fauna (CAFF). Retrieved from https://oaarchive.arctic-council.org/handle/11374/232

Merlis, T. M. (2014). Interacting components of the top-of-atmosphere energy balance affect changes in regional surface temperature. *Geophysical Research Letters*, *41*(20), 7291–7297. https://doi.org/10.1002/2014GL061700

Merlis, T. M., & Henry, M. (2018). Simple Estimates of Polar Amplification in Moist Diffusive Energy Balance Models. *Journal of Climate*, *31*(15), 5811–5824. https://doi.org/10.1175/JCLI-D-17-0578.1

Moon, T. A., Druckenmiller, M. L., & Thoman, R. L. (2021). NOAA Arctic Report Card 2021 Executive Summary. https://doi.org/10.25923/5S0F-5163

National Snow & Ice Data Center. (2020, May 4). Arctic People. Retrieved May 9, 2022, from https://nsidc.org/cryosphere/arctic-meteorology/arctic-people.html

Pithan, F., & Mauritsen, T. (2014). Arctic amplification dominated by temperature feedbacks in contemporary climate models. *Nature Geoscience*, *7*(3), 181–184. https://doi.org/10.1038/ngeo2071

Previdi, M., Janoski, T. P., Chiodo, G., Smith, K. L., & Polvani, L. M. (2020). Arctic Amplification: A Rapid Response to Radiative Forcing. *Geophysical Research Letters*, *47*(17), e2020GL089933. https://doi.org/10.1029/2020GL089933

Previdi, M., Smith, K. L., & Polvani, L. M. (2021). Arctic amplification of climate change: a review of underlying mechanisms. *Environmental Research Letters*, *16*(9), 093003. https://doi.org/10.1088/1748-9326/ac1c29

Raval, A., & Ramanathan, V. (1989). Observational determination of the greenhouse effect. *Nature*, *342*(6251), 758–761. https://doi.org/10.1038/342758a0

Rigor, I. G., Wallace, J. M., & Colony, R. L. (2002). Response of Sea Ice to the Arctic Oscillation. *Journal of Climate*, *15*(18), 2648–2663. https://doi.org/10.1175/1520-0442(2002)015<2648:ROSITT>2.0.CO;2

Russotto, R. D., & Biasutti, M. (2020). Polar Amplification as an Inherent Response of a Circulating Atmosphere: Results From the TRACMIP Aquaplanets. *Geophysical Research Letters*, *47*(6), e2019GL086771. https://doi.org/10.1029/2019GL086771

Screen, J. A., & Simmonds, I. (2010). The central role of diminishing sea ice in recent Arctic temperature amplification. *Nature*, *464*(7293), 1334–1337. https://doi.org/10.1038/nature09051

Screen, J. A., Deser, C., Simmonds, I., & Tomas, R. (2014). Atmospheric impacts of Arctic sea-ice loss, 1979–2009: separating forced change from atmospheric internal variability. *Climate Dynamics*, *43*(1), 333–344. https://doi.org/10.1007/s00382-013-1830-9

Serreze, M. C., Barrett, A. P., Stroeve, J. C., Kindig, D. N., & Holland, M. M. (2009). The emergence of surface-based Arctic amplification. *The Cryosphere*, *3*(1), 11–19. https://doi.org/10.5194/tc-3-11-2009

Shell, K. M., Kiehl, J. T., & Shields, C. A. (2008). Using the Radiative Kernel Technique to Calculate Climate Feedbacks in NCAR's Community Atmospheric Model. *Journal of Climate*, *21*(10), 2269–2282. https://doi.org/10.1175/2007JCLI2044.1

Singh, H. A., Rasch, P. J., & Rose, B. E. J. (2017). Increased Ocean Heat Convergence Into the High Latitudes With CO2 Doubling Enhances Polar-Amplified Warming. *Geophysical Research Letters*, *44*(20), 10,583-10,591. https://doi.org/10.1002/2017GL074561

Smith, D. M., Eade, R., Andrews, M. B., Ayres, H., Clark, A., Chripko, S., et al. (2022). Robust but weak winter atmospheric circulation response to future Arctic sea ice loss. *Nature Communications*, *13*(1), 727. https://doi.org/10.1038/s41467-022-28283-y

Smith, Doug M., Screen, J. A., Deser, C., Cohen, J., Fyfe, J. C., García-Serrano, J., et al. (2019). The Polar Amplification Model Intercomparison Project (PAMIP) contribution to CMIP6: investigating the causes and consequences of polar amplification. *Geoscientific Model Development*, *12*(3), 1139–1164. https://doi.org/10.5194/gmd-12-1139-2019

Soden, B. J., Held, I. M., Colman, R., Shell, K. M., Kiehl, J. T., & Shields, C. A. (2008). Quantifying Climate Feedbacks Using Radiative Kernels. *Journal of Climate*, *21*(14), 3504–3520. https://doi.org/10.1175/2007JCLI2110.1

Stroeve, J. C., Serreze, M. C., Holland, M. M., Kay, J. E., Malanik, J., & Barrett, A. P. (2012). The Arctic's rapidly shrinking sea ice cover: a research synthesis. *Climatic Change*, *110*(3), 1005–1027. https://doi.org/10.1007/s10584-011-0101-1

Stuecker, M. F., Bitz, C. M., Armour, K. C., Proistosescu, C., Kang, S. M., Xie, S.-P., et al. (2018). Polar amplification dominated by local forcing and feedbacks. *Nature Climate Change*, *8*(12), 1076–1081. https://doi.org/10.1038/s41558-018-0339-y

Swart, N. C., Fyfe, J. C., Hawkins, E., Kay, J. E., & Jahn, A. (2015). Influence of internal variability on Arctic sea-ice trends. *Nature Climate Change*, *5*(2), 86–89. https://doi.org/10.1038/nclimate2483

Vavrus, S. J., Bhatt, U. S., & Alexeev, V. A. (2011). Factors Influencing Simulated Changes in Future Arctic Cloudiness. *Journal of Climate*, *24*(18), 4817–4830. https://doi.org/10.1175/2011JCLI4029.1

Wang, Q., Fan, X., & Wang, M. (2016). Evidence of high-elevation amplification versus Arctic amplification. *Scientific Reports*, *6*(1), 19219. https://doi.org/10.1038/srep19219

Winton, M. (2006). Amplified Arctic climate change: What does surface albedo feedback have to do with it? *Geophysical Research Letters*, *33*(3). https://doi.org/10.1029/2005GL025244

Yang, W., & Magnusdottir, G. (2018). Year-to-year Variability in Arctic Minimum Sea Ice Extent and its Preconditions in Observations and the CESM Large Ensemble Simulations. *Scientific Reports*, *8*(1), 9070. https://doi.org/10.1038/s41598-018-27149-y

Zhang, R., Wang, H., Fu, Q., Pendergrass, A. G., Wang, M., Yang, Y., et al. (2018). Local Radiative Feedbacks Over the Arctic Based on Observed Short-Term Climate Variations. *Geophysical Research Letters*, *45*(11), 5761–5770. https://doi.org/10.1029/2018GL077852

Zubrzycki, S., Kutzbach, L., & Pfeiffer, E.-M. (2014). Permafrost-affected soils and their carbon pools with a focus on the Russian Arctic. *Solid Earth*, *5*(2), 595–609. https://doi.org/10.5194/se-5-595-2014